

- [1-hydroxy-1-(2-nitro-4,5-methylenedioxyphenyl)-methyl-phenoxyl]-2-(2'-amino-5'-methylphenoxyl)-ethane-*N,N,N',N'*-tetraacetic acid; Calbiochem] [J. P. Y. Kao, A. T. Harootian, R. Y. Tsien, *J. Biol. Chem.* **264**, 8179 (1989)]. On the assumption that a brief depolarization-induced increase in cytosolic Ca^{2+} loads nitr-5 with Ca^{2+} , the cells were then bathed in saline containing 20 mM K^{+} for 10 s. Myocytes loaded with nitr-5-AM were transferred to the recording chamber containing untreated *Xenopus* nerve-muscle cultures. Cell manipulation was performed as previously described (14).
11. The distance refers to the center-to-center distance between the spherical myocytes. The diameter of the myocytes was $29 \pm 7 \mu\text{m}$ (mean \pm SEM, $n = 50$). Physical contact between the two myocytes was avoided because these cells undergo electrical coupling after contact in culture [M. Chow and M.-m. Poo, *J. Physiol. (London)* **346**, 181 (1984)].
 12. Photolysis of nitr-5 in loaded myocytes was induced with a 2-s pulse of steady light from a 75-W xenon lamp. The light passed through a UG1 filter, a dichroic mirror (XFO 400; DCLP), a 40 \times water immersion objective, and a no. 1 cover glass before reaching the cell. The photolysis efficiency of the light source through the microscope was 14 and 42% per second for Ca^{2+} -free and Ca^{2+} -bound nitr-5, respectively [R. S. Zucker, *Cell Calcium* **14**, 87 (1993)] (8). Assuming that nitr-5 accumulated in cells to ~ 1 mM and was 40% loaded with Ca^{2+} , so that the free intracellular Ca^{2+} concentration remained at 100 nM, we calculated that a 2-s UV exposure increases the Ca^{2+} concentration to ~ 320 nM, with a half-time of decay of ~ 15 s and with extrusion slowed by the extra buffering provided by nitr-5 [L. Landó and R. S. Zucker, *J. Neurophysiol.* **72**, 825 (1989)]. We have observed a larger photolysis-induced increase in Ca^{2+} by direct Ca^{2+} imaging with the fluorescent dye fluo-3 in separate myocyte cultures and with a 10-s UV light exposure through the same optics.
 13. Synaptic currents were recorded from innervated muscle cells by whole-cell recording methods [O. P. Hamill, A. Marty, E. Neher, B. Sakmann, F. J. Sigworth, *Pflügers Arch.* **391**, 85 (1981); S. H. Young and M.-m. Poo, *Nature* **305**, 634 (1983)] with a patch-clamp amplifier (Axopatch 1D; Axon Instruments). The solution inside the recording pipette contained 150 mM KCl, 1 mM NaCl, 1 mM MgCl_2 , and 10 mM Hepes (pH 7.2). Recordings were made at room temperature in Hepes-buffered Ringer's solution, to which B27 supplement [1:100 (v/v); Gibco] was added to provide antioxidants to help prevent UV-induced cell damage. Extracellular stimulation of the presynaptic neuron was achieved with a patch electrode at the cell body under loose-seal conditions. The recorded membrane current was filtered at 1 kHz and stored on videotape, for later playback on a storage oscilloscope (TDS320; Tektronix) or an oscillographic recorder (TA240; Gould) and for analysis by computer with the SCAN program (J. Dempster, University of Strathclyde, Glasgow, UK).
 14. Z. Xie and M.-m. Poo, *Proc. Natl. Acad. Sci. U.S.A.* **83**, 7069 (1986); J. Evers, M. Laser, Y. Sun, Z.-p. Xie, M.-m. Poo, *J. Neurosci.* **9**, 1523 (1989).
 15. The site of innervation on spherical myocytes is centrally located on the substrate-facing surface and not at the apparent perimeter of the myocyte (6). Therefore, distances between the two myocytes were obtained by measuring the distance between the centers of the two myocytes along the neurite. Two myocytes may be located on the same neurite without branches, on two different branches of the same neurite, or on two different neurites, regardless of their relative distances from the cell body.
 16. Local perfusion of culture medium was achieved with a large suction micropipette (inner diameter, 10 to 20 μm) connected by means of fluid-filled tubing to a fluid reservoir. The suction or outflow pressure was adjusted by changing the level of the fluid reservoir relative to that of the culture dish. The flow pattern was tested before the experiment with medium containing trypan blue (Fig. 4B) and was monitored during the experiment by observing the movement of small cell debris in the culture.
 17. The rate of diffusion along the neurite can be estimated by the equation $s^2 = 2Dt$, where s is the average distance of diffusion over time t , and D is the diffusion coefficient. For a globular protein of 45 kD, such as ovalbumin, the diffusion coefficient in these *Xenopus* neurites was $15.8 \pm 2.1 \mu\text{m}^2/\text{s}$ [S. Popov and M.-m. Poo, *J. Neurosci.* **12**, 77 (1992)]. Thus, the average time required for diffusion of a cytosolic protein of 45 kD over a distance of 150 to 200 μm is ~ 12 to 20 min. Simple diffusional signaling between the synapses could thus account for the delay in the onset of synaptic depression observed at distant sites. Active retrograde transport could achieve a rate of 30 to 180 $\mu\text{m}/\text{min}$ [R. D. Allen, J. Metzuzals, I. Tasaki, S. T. Brady, S. P. Gilbert, *Science* **218**, 1127 (1982)], allowing more rapid signaling than diffusion.
 18. The cytosolic signal that mediates the spread of depression should be distinguished from the initial retrograde signal provided by the postsynaptic myocyte after the increase in cytosolic Ca^{2+} , the nature of which remains obscure. In principle, the latter could be a membrane-permeant diffusible signal that acts locally at the synapse. Alternatively, the signal may be mediated by membrane-bound surface molecules that act across the synaptic cleft. Evidence suggests that nitric oxide (NO) may mediate a presynaptic modulation of transmitter secretion induced by long-term repetitive postsynaptic depolarizations at *Xenopus* neuromuscular junctions [T. Wang, Z. Xie, B. Lu, *Nature* **374**, 262 (1995)]. Our attempts to demonstrate a role for NO in heterosynaptic or ACh-induced synaptic depression, which may involve mechanisms distinct from those activated by long-term repetitive depolarizations, have so far been unsuccessful.
 19. R. Horn and A. Marty, *J. Gen. Physiol.* **92**, 145 (1988).
 20. Supported by grants from NSF (IBN 22106) to M.-m.P. and NIH (NS 15114) to R.S.Z.

13 November 1995; accepted 22 February 1996

Structures of an MHC Class II Molecule with Covalently Bound Single Peptides

Daved H. Fremont,* Wayne A. Hendrickson, Philippa Marrack, John Kappler

The high-resolution x-ray crystal structures of the murine major histocompatibility complex (MHC) class II molecule, I-E^k, occupied by either of two antigenic peptides were determined. They reveal the structural basis for the I-E^k peptide binding motif and suggest general principles for additional alleles. A buried cluster of acidic amino acids in the binding groove predicted to be conserved among all murine I-E and human DR MHC class II molecules suggests how pH may influence MHC binding or exchange of peptides. These structures also complement mutational studies on the importance of individual peptide residues to T cell receptor recognition.

Antigen presentation by MHC class II molecules involves the intracellular generation of antigen peptide fragments, their binding to MHC molecules, and the transport of the complexes to the cell surface for recognition by the $\alpha\beta$ T cell receptor (TCR) of CD4⁺ T cells (1, 2). Although MHC molecules bind peptides promiscuously, there often is a characteristic peptide binding motif for each MHC allele controlled by a few of the peptide amino acids (3, 4). We have produced a number of soluble murine I-E^k molecules, each of which is homogeneously occupied by a different peptide tethered by means of a flexible protein linker to the NH₂-terminus of the β chain (5–7). Several of these proteins crystallized readily. Two yielded crystals suitable for x-ray diffraction analysis (8):

one was occupied by a peptide derived from murine hemoglobin [Hb(64–76)] (9) and a second with a peptide from murine heat shock protein 70 [Hsp(236–248)] (10). The structures of these complexes (Fig. 1) were determined at 2.3 Å and 2.7 Å resolution, respectively (11–13).

The peptides, well resolved in both structures, are bound in a groove between the α helices of the MHC $\alpha 1$ and $\beta 1$ domains, with both the NH₂- and COOH-termini of the peptides protruding from the ends of the groove. The path of the flexible linkers from the NH₂-termini of the peptides to the COOH-terminus of the $\beta 1$ domain avoids the upper surface of the molecules, which accounts for their lack of interference in TCR recognition (5, 14). The two I-E^k structures are similar to each other and, with the exception of minor backbone variations, to that of two human DR peptide structures, DR1 complexed with an influenza hemagglutinin peptide [HA(306–318)] (15) and DR3 complexed with the invariant chain CLIP peptide (16).

Despite the fact that the two I-E^k-peptide complexes crystallized in different lattices, the asymmetric unit in both cases was the same dimer of $\alpha\beta$ heterodimers. However, the geometry of this dimer is different from that of the dimer seen in the DR1 and

D. H. Fremont, Howard Hughes Medical Institute, Department of Biochemistry and Molecular Biophysics, Columbia University, New York, NY 10032, USA, and Howard Hughes Medical Institute, Division of Basic Immunology, National Jewish Center for Immunology and Respiratory Medicine, Denver, CO 80206, USA.
W. A. Hendrickson, Howard Hughes Medical Institute, Department of Biochemistry and Molecular Biophysics, Columbia University, New York, NY 10032, USA.
P. Marrack and J. Kappler, Howard Hughes Medical Institute, Division of Basic Immunology, National Jewish Center for Immunology and Respiratory Medicine, Denver, CO 80206, USA.

*To whom correspondence should be addressed.

DR3 crystals (15–18) (Fig. 2). It has been speculated that the DR dimer has biological significance, because it can be anchored in the membrane in an upright position with sites for the TCR, superantigen, and CD4 interaction exposed (17). Although these sites are exposed on the I-E^k dimers as well, the outwardly pointing $\alpha 2$ and $\beta 2$ domains would require these molecules to lie nearly flat on the membrane surface. It is difficult to speculate about the functional relevance of the I-E^k dimers, because the nonphysiological peptide linker forms part of the dimer interface. It is worth noting that neither the position of this linker nor the exposed I-E^k amino acids would appear to preclude the existence of a DR-like dimer for the I-E^k molecules. The possibility remains that both the I-E^k and DR dimers are artifacts of the conditions used to obtain crystals, which for both molecules included high concentrations of polyethylene glycol and low pH.

Two types of interactions contribute to the binding of the peptides to I-E^k. First, there is a network of hydrogen bonds between amino acids of I-E^k and the peptide backbones; this network is similar in both I-E^k complexes and in the DR1-HA and DR3-CLIP structures. This network also imparts a polyproline II helix-like structure on the peptides (15). One unique aspect of the I-E^k structures is an additional hydrogen bond from the peptide P2 side chain (Hb-Thr^{P2} and Hsp-Asn^{P2}) to the carbonyl of Thr⁷⁷ of the β chain (Thr⁷⁷), which interdigitates into the β chain α helix. Second, the side chains of peptide residues P1, P4, P6, and P9 are buried into deep pockets of both I-E^k structures (Fig. 3). The P1 pocket is medium-sized and hydrophobic, accepting the side chain of either Hb-Ile^{P1} or Hsp-Val^{P1}. The side chain of Phe^{P4} of both peptides is buried in a significantly larger, predominantly hydrophobic pocket. A hydrophilic pocket accepts the Hb-Glu^{P6} side chain. The smaller side chain of Hsp-Ala^{P6} results in the filling of this pocket with water molecules. Finally, the P9 pocket is a narrow hydrophobic tunnel with Glu^{P9} at its base, to which Lys^{P9} of both peptides forms a salt bridge. The structure of these pockets provides an explanation of the motifs for a large number of I-E^k binding peptides (3, 9, 10, 19, 20). Nearly all of these peptides have an Ile, Leu, or Val residue at P1 and a Lys (or occasionally Arg) at P9. The pockets for P4 and P6 are less restrictive, although hydrophobic amino acids predominate at P4, and Gln, Asp, or Asn residues are common at P6.

A comparison of I-E and DR sequences and structures suggests that a few key variable amino acids in the β chain determine the shape and specificity of the pockets. The α chain amino acids contributing to the I-E^k

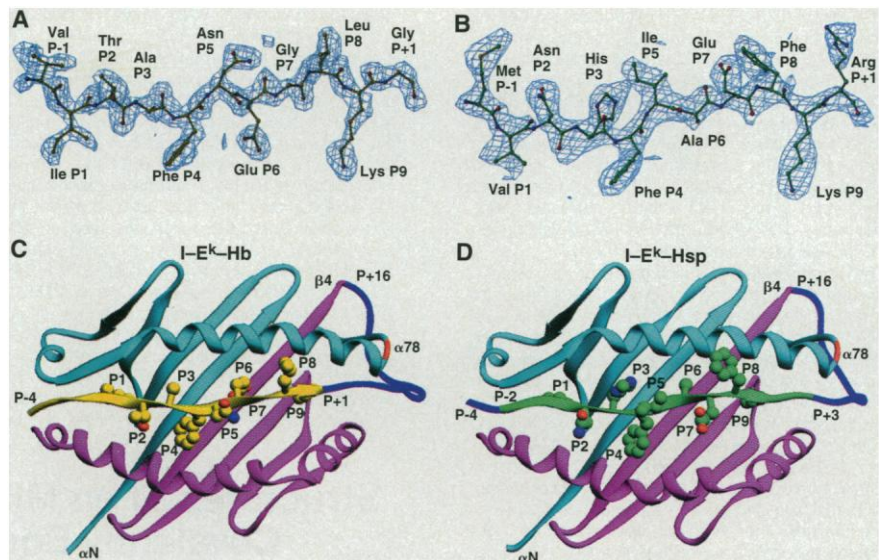


Fig. 1. Structure of two peptides covalently bound to I-E^k (11–13). **(A)** Residues P1 to P9 [mouse Hb(68–76)] of the I-E^k-Hb complex at 2.3 Å. **(B)** Residues P1 to P9 [mouse Hsp70(238–246)] of the I-E^k-Hsp complex at 2.7 Å. Both electron density maps were calculated with $(|F_o| - |F_c|) \exp(i\phi_c)$ coefficients, where F_o is the observed structure factor and F_c and ϕ_c are the model structure factor and phase, respectively, calculated in the absence of the respective fragments. These omit maps are displayed as map covers contoured at 2σ . **(C)** Ribbon (26) diagram of the I-E^k-Hb complex showing the $\alpha 1$ (cyan) and $\beta 1$ (magenta) domains and the path of the Hb peptide (yellow) and linker (blue). Peptide side chains P1 to P9 are displayed in yellow. **(D)** Ribbon diagram of I-E^k-Hsp with Hsp in green.

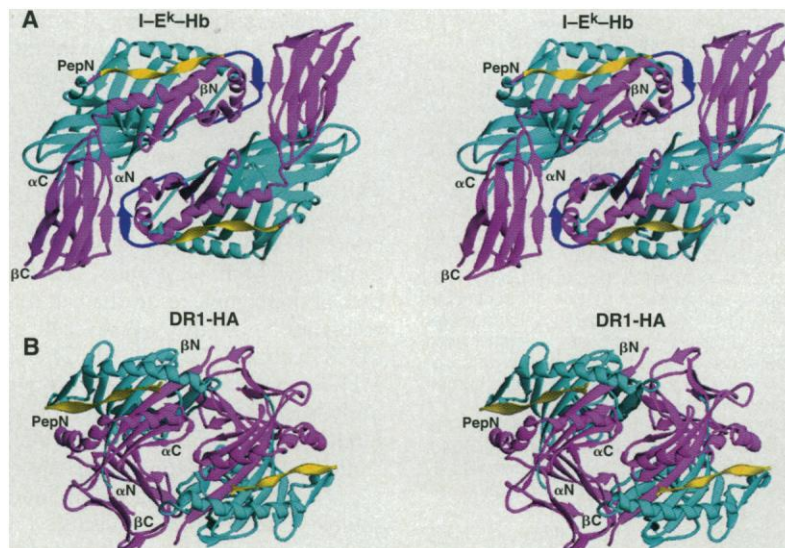


Fig. 2. Comparison of the crystallographically observed I-E^k **(A)** and DR1 dimers **(B)**. A stereoscopic ribbon (26) diagram of I-E^k-Hb is shown with the E α^d chain in cyan, E β^k in magenta, the core of the Hb peptide in yellow, and the linker region in blue. For comparison, a DR1 dimer is shown with the same color scheme. Each dimer of heterodimers is shown looking down its noncrystallographic twofold axis. An average of 792 Å² of solvent-accessible area (27) is buried in the dimer interface for each I-E^k-Hb complex, compared to 774 Å² for I-E^k-Hsp and 783 Å² for DR1-HA (28).

peptide binding pockets are virtually identical to those used in DR1 and DR3. In the P1 pocket, a small β chain residue at position 86 allows for large aromatic P1 side chains (that is, Gly⁸⁶ in DR1 and Ser⁸⁶ in I-E^d) (15, 20), whereas Phe⁸⁶ in the I-E^k P1 pocket selects for smaller hydrophobic residues. Compared to I-E^k, the P4 and P6 pockets of DR1 are significantly truncated and redirected as a result of a few differences in the β

chain (for example, $\beta 11$, $\beta 13$, $\beta 30$, $\beta 74$, and $\beta 78$). I-E peptide binding motifs have little sequence restriction at P7, as the surface pocket found in DR1 is filled by two aromatic residues ($\beta 30$ and $\beta 67$) in all I-E alleles. In the P9 pocket, Glu⁸⁹ in I-E^k, I-E^d, I-E^s, and I-E^b explains the peptide preference of Lys (or Arg) for these alleles, whereas a Trp⁸⁹ in DR1 creates a shorter, hydrophobic pocket.

These structures are helpful in under-

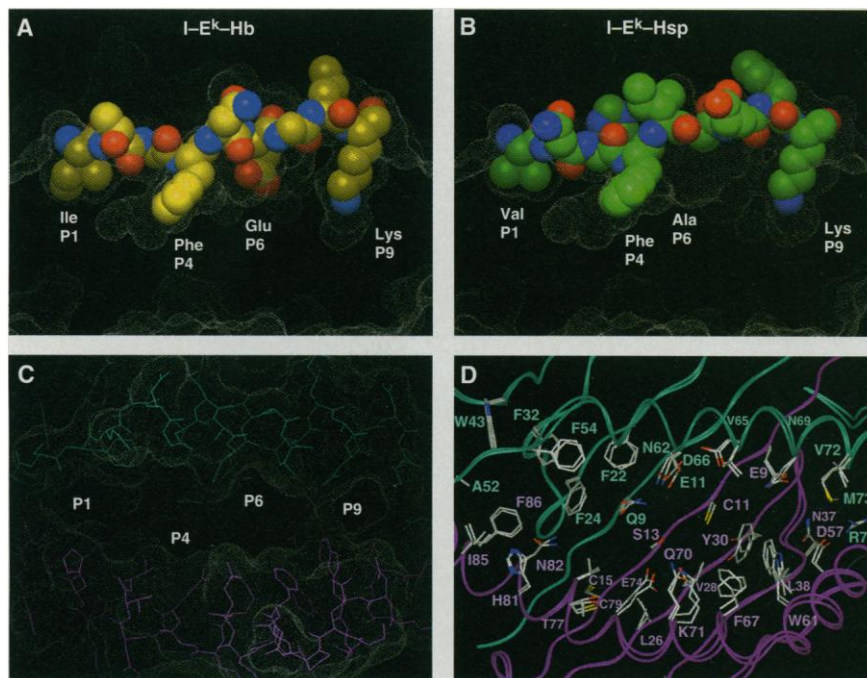
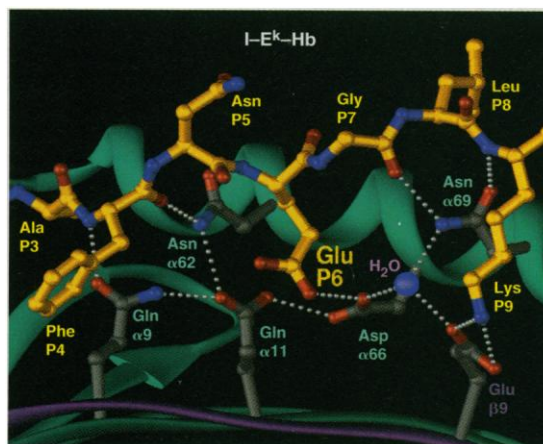


Fig. 3. Specificity of the I-E^k peptide binding pockets. **(A)** Side view of the I-E^k-Hb complex with part of the β chain α helix cut away, showing the fit of the peptide into individual pockets of the class II groove. The solvent-accessible surface of I-E^k is represented as gray dots, and the Hb peptide carbon atoms are shown in yellow, except for oxygen (red) and nitrogen (blue). **(B)** An identical side view of the I-E^k-Hsp complex, with the Hsp peptide carbon atoms shown in green. **(C)** Top view of the I-E^k binding groove (Hb complex) without the peptide, with a stick structure for the α chain in cyan and the β chain in magenta. **(D)** Superimposed ribbons of the two I-E^k binding platforms with all side chains that lose appreciable solvent-accessible surface in either peptide complex displayed and labeled. Residues P1 to P9 of the Hb peptide are 79.6% buried (696 Å²) in the I-E^k groove, whereas 69.1% (647 Å²) of the Hsp peptide becomes inaccessible to a 1.4 Å probe sphere. The fractional buried areas for each side chain of Hb and Hsp, respectively, are as follows: P1 (1.00, 1.00); P2 (0.58, 0.59); P3 (0.84, 0.70); P4 (1.00, 0.97); P5 (0.60, 0.25); P6 (0.99, 0.84); P7 (Gly, 0.62); P8 (0.37, 0.31); and P9 (1.00, 1.00).

Fig. 4. Hydrogen bonding network in the P6 pocket. The putative hydrogen bonds (silver balls) between the Hb peptide (yellow) and I-E^k (α in cyan and β in magenta) are shown. This scheme requires that two of the three carboxylate groups in the P6 pocket are protonated (Glu ^{α 11}, Asp ^{α 66}, and Glu^{P6}). The five α chain residues that participate in the hydrogen-bonding network (α 9, α 11, α 62, α 66, and α 69) are conserved in all I-E and DR1 alleles, as are their conformations in the I-E^k-Hb, I-E^k-Hsp, DR1-HA, and DR3-CLIP complexes. The water molecule adjacent to Asp ^{α 66} is likewise conserved. Therefore, it would appear that the primary variation of this hydrogen-bonding scheme would be associated with β chain polymorphisms (for example, β 9, β 11, β 13, and β 30), as they serve to select the preferred residues that bind into the P6 and P9 pockets.



standing the role of individual peptide amino acids in the TCR recognition of the I-E^k-peptide complexes. For example, Hb-Asn^{P5} points straight up from the middle of the peptide binding groove and interacts with Gln ^{β 70} at the protein surface (Figs. 1C and 3A). Mutations at this position disrupt TCR recognition for nearly all I-E^k-Hb-reactive T cell clones (9). Likewise, in an

I-E^k-presented peptide derived from moth cytochrome c [Mcc(91-103)] a Lys residue, predicted to lie at position P5, has been shown to be critical for TCR recognition and is usually matched by an acidic residue in CDR3 of the TCR α chain (19, 21). In addition, mutations at P5 and other solvent-exposed amino acids (P2, P3, P7, and P8) of the Hb and Mcc peptides either

disrupt TCR interaction or result in an altered recognition that sometimes antagonizes T cell activation by a wild-type peptide-MHC ligand (22). Similar structural observations have been made for antagonist peptide-MHC class I complexes (23). Interestingly, the mutation of P6 from Glu to Asp in the Hb peptide generates one of these antagonizing altered peptide ligands, despite the fact that the side chain of P6 is deeply buried in a binding pocket (Figs. 3A and 4). If the Asp side chain were to maintain an equivalent interaction as Glu in the P6 pocket, the local conformation of the solvent-exposed regions would necessarily be changed, accounting for the altered TCR recognition. In fact, although the peptide backbone positions are similar for Hb, Hsp, HA, and CLIP, the greatest variation is in the vicinity of P5 and P6, where main chain deviations greater than 1.0 Å are evident.

The P6 pocket contains one of the most unexpected features observed in the I-E^k complexes. Here, two acidic amino acids of the class II molecule (Glu ^{α 11} and Asp ^{α 66}) face each other. The local geometry indicates that these carboxylic acids are protonated and stabilized by a network of hydrogen bonds with a conserved water molecule and surrounding amino acids (Fig. 4). Because these two amino acids are conserved in all I-E and DR molecules, a similar network is likely to be a common feature of most alleles. In the I-E^k-Hb complex, a third acidic amino acid, Glu^{P6}, is introduced into this network. It is well established that I-E and DR peptide loading or exchange are favored by a low pH, such as that found in the endosomal compartment where peptide loading naturally occurs (1, 24). It is tempting to suggest that this is related to a need to protonate these acidic amino acids before complex formation. Indeed, data from a preliminary electrostatic calculation indicate that the pK_a's of all three P6 pocket carboxylate groups in the I-E^k-Hb complex are increased relative to their solution values (25). Once the peptide is ensconced in the binding groove, these now-protonated carboxylate groups are protected from the solvent and the structure can be stable at the neutral pH of the cell surface. One role of this pH dependency may be to ensure cellular specificity of peptide presentation by reducing the possibility of peptide loading outside the proper intracellular compartments.

REFERENCES AND NOTES

1. R. N. Germain and D. H. Margulies, *Annu. Rev. Immunol.* **11**, 403 (1993).
2. P. Cresswell, *ibid.* **12**, 259 (1994).
3. V. Brusica, G. Rudy, L. Harrison, *Nucleic Acids Res.* **22**, 3663 (1994).
4. H. G. Rammensee, *Curr. Opin. Immunol.* **7**, 85 (1995).
5. H. Kozono, J. White, J. Clements, P. Marrack, J. Kappler, *Nature* **369**, 151 (1994).
6. H. Kozono, D. Parker, J. White, P. Marrack, J. Kap-

- pler, *Immunity* **3**, 187 (1995).
- Covalent complexes of I-E^k-Hb and I-E^k-Hsp were produced as soluble heterodimers in insect cells with a baculovirus expression system (5, 6). Secreted class II molecules were immunopurified from culture supernatants with the I-E^k antibody 14-4-4, followed by size exclusion chromatography with Superdex-200 (Pharmacia).
 - We grew crystals of I-E^k-Hb and I-E^k-Hsp of data collection quality by equilibrating 5 to 10 mg/ml of purified protein against 16 to 18% polyethylene glycol 4000 (Fluka), 2% ethylene glycol, 200 mM ammonium sulfate, and 100 mM citrate (pH 5.2 to 5.6). Crystals were cryoprotected by the addition of 20% polyethylene glycol 4000, 20% ethylene glycol, and 10% glycerol.
 - B. D. Evavold, S. G. Williams, B. L. Hsu, S. Buus, P. M. Allen, *J. Immunol.* **148**, 347 (1992).
 - M. Marrack, L. Ignatowicz, J. W. Kappler, J. Boymel, J. H. Freed, *J. Exp. Med.* **178**, 2173 (1993).
 - Crystals were cryopreserved in a -160°C nitrogen stream, and data were collected at the HHMI X-4A beamline of the National Synchrotron Light Source at Brookhaven National Laboratory. For I-E^k-Hb, data were measured from two crystals at wavelengths of 0.9879 Å and 1.0070 Å, whereas x-rays of 0.9789 Å wavelength were used on a single crystal of I-E^k-Hsp. Data were collected on Fuji imaging plates for 2 to 4 min with 2° oscillation ranges. These data were autoindexed and processed with DENZO [Z. Otwinowski, L. Sawyer, N. Isaacs, S. Bailey, Eds. (SERC Daresbury Laboratory, Warrington, UK, 1993), pp. 56], scaled with SCALA, and merged with AGROVATA (SERC Collaborative Computing Project No. 4, Daresbury Laboratory, Warrington, UK, 1979). The I-E^k-Hb crystals belong to space group C2 with unit cell dimensions $a = 147.0 \text{ \AA}$, $b = 57.1 \text{ \AA}$, $c = 117.0 \text{ \AA}$, and $\beta = 91.5^\circ$. A total of 169,034 observations were merged to 38,809 reflections with an $R_{\text{sym}} = 0.075$ and 89.2% completion between 20 and 2.3 Å. $R_{\text{sym}} = \sum |I - \langle I \rangle| / \sum I$, where I is the observed intensity and $\langle I \rangle$ is the average intensity obtained from multiple observations of symmetry-related reflections. The I-E^k-Hsp crystals belong to space group P3₂1 with unit cell dimensions $a = b = 77.6 \text{ \AA}$ and $c = 319.6 \text{ \AA}$. A total of 85,623 observations were merged to 29,069 reflections with an $R_{\text{sym}} = 0.087$ and 92.1% completion between 20 and 2.7 Å. The solvent contents are 55% and 60% for the respective crystals with two heterodimeric complexes per asymmetric unit.
 - Phases for the I-E^k-Hb data were obtained by molecular replacement with the coordinates of a single HLA-DR1 heterodimer (15) with mismatched amino acid residues replaced with Ala side chains. AMORE [J. Navaza, *Acta Crystallogr.* **50**, 157 (1994)] rotation and translation function results were unambiguous for two heterodimers in the asymmetric unit. The molecular replacement structure of I-E^k-Hsp was solved with a single heterodimer of the partially refined I-E^k-Hb. After rigid body refinement, the R factors for I-E^k-Hb and I-E^k-Hsp were 43% and 37%, respectively, for data from 8 to 3 Å.
 - Model building was carried out with a modified version of TOM/FRODO [T. A. Jones, *J. Appl. Crystallogr.* **11**, 268 (1978)]. Minimization and simulated annealing refinements were carried out with X-PLOR [A. Brunger, X-PLOR, version 3.1 manual (Yale Univ. Press, New Haven, 1992)], which used noncrystallographic symmetry restraints. For I-E^k-Hb, the current model for each half of the dimer contains 182 residues of I-E α^d ($\alpha 1$ to $\alpha 182$), 13 mouse Hb(64-76) residues (P-4 to P-9), 16 linker residues (P+1 to P+16) connecting to 185 residues of the natural I-E β^k ($\beta 4$ to $\beta 188$), and 3 carbohydrates N-linked to Asn^{N78}, Asn^{N118}, and Asn^{P19}. There are 349 water molecules in the dimer for a total of 6773 nonhydrogen atoms. The R value stands at 21.1% for all data from 6 to 2.3 Å with an R_{free} of 28.5% (for data greater than 2σ , $R = 20.8\%$ and $R_{\text{free}} = 28.2\%$). The average atomic temperature factor is 32.3 Å², and the model has root-mean-square (rms) deviations of 0.010 Å and 1.63° from ideal bond lengths and angles, respectively. The I-E^k-Hb complexes can be superimposed with an rms deviation of 0.35 Å. For I-E^k-Hsp, the current model for each complex contains 182 residues of I-E α^d ($\alpha 1$ to $\alpha 182$), 2 residues NH₂-terminal to the peptide (P-4 to P-3), 13 mouse Hsp70 (236 to 248) residues (P-2 to P+2), 14 linker residues (P+3 to P+16) connecting to 185 residues of the natural I-E β^k ($\beta 4$ to $\beta 188$), and 3 carbohydrates. There are 159 water molecules and 1 sulfate ion for a total of 6676 nonhydrogen atoms. The R value stands at 23.3% for all data from 6 to 2.3 Å with an R_{free} value of 33.4% (for data greater than 2σ , the $R = 22.2\%$ and $R_{\text{free}} = 32.1\%$), with an average temperature factor of 36.5 Å² and rms deviations of 0.011 Å and 1.73° from ideal bond lengths and angles, respectively. The two I-E^k-Hsp complexes compare favorably with an rms deviation of 0.37 Å. For both models, no attempt was made to build the peptide NH₂-terminal regions (P-8 to P-5 of Hb and P-7 to P-5 of Hsp) or the COOH-terminal 10 residues of either the α or β chains, as these regions appear highly disordered in the electron density maps. The density for residues $\beta 107$ to $\beta 113$ was poor in both peptide complexes; this segment is modeled as polyalanine.
 - L. Ignatowicz, G. Winslow, J. Bill, J. Kappler, P. Marrack, *J. Immunol.* **154**, 3852 (1995).
 - L. J. Stern *et al.*, *Nature* **368**, 215 (1994).
 - P. Ghosh, M. Amaya, E. Mellins, D. C. Wiley, *ibid.* **378**, 457 (1995).
 - J. H. Brown *et al.*, *ibid.* **364**, 33 (1993).
 - T. S. Jardetzky *et al.*, *ibid.* **368**, 711 (1994).
 - P. A. Reay, R. M. Kantor, M. M. Davis, *J. Immunol.* **152**, 3946 (1994).
 - H. Schild *et al.*, *Int. Immunol.* **7**, 1957 (1995).
 - J. L. Jorgensen, U. Esser, B. F. de St. Groth, P. A. Reay, M. M. Davis, *Nature* **355**, 224 (1992).
 - B. D. Evavold and P. M. Allen, *Science* **252**, 1308 (1991); B. D. Evavold, J. Sloan-Lancaster, B. L. Hsu, P. M. Allen, *J. Immunol.* **150**, 3131 (1993); L. M. Spain, J. L. Jorgensen, M. M. Davis, L. J. Berg, *ibid.* **152**, 1709 (1994).
 - D. H. Fremont *et al.*, *Proc. Natl. Acad. Sci. U.S.A.* **92**, 2479 (1995).
 - P. E. Jensen, *J. Exp. Med.* **171**, 1779 (1990); A. Sette *et al.*, *J. Immunol.* **148**, 844 (1992); J. Boniface *et al.*, *Biochemistry* **32**, 11761 (1993); P. Reay, D. Wettstein, M. M. Davis, *EMBO J.* **11**, 2829 (1992).
 - Nir Ben-Tal, D. H. Fremont, A. Windemuth, W. A. Hendrickson, B. Honig, unpublished results. The pK_a is the negative logarithm of the acid constant.
 - M. Carson, *J. Mol. Graphics* **5**, 103 (1987).
 - M. L. Connolly, *ibid.* **3**, 19 (1985). Solvent-accessible surface calculations were performed with a 1.4 Å probe sphere.
 - The following residues make at least one contact ($\leq 4.0 \text{ \AA}$) in either the I-E^k-Hb or I-E^k-Hsp dimer interface: Lys^{N2}, Glu^{N4}, Asp^{N141}, Tyr^{B18}, Arg^{B23}, Arg^{B25}, Arg^{B39}, Asp^{B41}, Asp^{B43}, Val^{B44}, Arg^{B48}, Val^{B50}, Glu^{B52}, Arg^{B55}, Lys^{B139}, Thr^{B140}, Gly^{B141}, Ile^{B142}, Val^{B143}, Ser^{B144}, Thr^{B145}, Gly^{B146}, Leu^{B147}, Met^{B160}, and the peptide linker residues Gly^{P+3}, Gly^{P+4}, Ser^{P+5}, Leu^{P+6}, and Val^{P+7}. In only the I-E^k-Hsp dimer is a sulfate ion found coincident with the noncrystallographic diad axis sequestered by four Arg residues (Arg^{B25} and Arg^{B29}). There is no obvious reason why a sulfate ion is not also present in the I-E^k-Hb crystal. Perhaps dimer packing in the different space groups, slight differences in pH, or small changes in the dimer interface controlled the sequestering of the sulfate ion. There is no obvious influence of the peptide or linker on sulfate coordination.
 - We thank J. Clements, F. Crawford, H. Kozono, D. Parker, and J. White for help in making the soluble class II molecules and H.-E. Aronson, K. Choi, C. Lima, X. Zhao, and X. Zhu for aid in the synchrotron data collection and Nir Ben-Tal for electrostatic discussions. Coordinates have been deposited in the Brookhaven Protein Data Bank (entries 1IEA and 1IEB) and are available via e-mail (fremont@columbia.edu).

14 November 1995; accepted 1 March 1996

Specification of Pituitary Cell Lineages by the LIM Homeobox Gene *Lhx3*

Hui Z. Sheng,* Alexander B. Zhdanov,*† Bedrich Mosinger Jr.,‡
Tetsuya Fujii,§ Stefano Bertuzzi,|| Alexander Grinberg,
Eric J. Lee, Sing-Ping Huang, Kathleen A. Mahon,¶
Heiner Westphal¶#

During pituitary organogenesis, the progressive differentiation of distinct pituitary-specific cell lineages from a common primordium involves a series of developmental decisions and inductive interactions. Targeted gene disruption in mice showed that *Lhx3*, a LIM homeobox gene expressed in the pituitary throughout development, is essential for differentiation and proliferation of pituitary cell lineages. In mice homozygous for the *Lhx3* mutation, Rathke's pouch formed but failed to grow and differentiate; such mice lacked both the anterior and intermediate lobes of the pituitary. The determination of all pituitary cell lineages, except the corticotrophs, was affected, suggesting that a distinct, *Lhx3*-independent ontogenetic pathway exists for the initial specification of this lineage.

Pituitary organ commitment occurs during the formation of Rathke's pouch, the ectodermal primordium of the anterior and intermediate lobes of the pituitary, when it comes in contact with neuroectoderm of the ventral hypothalamus (1). Inductive interactions between these tissues are required for their proper determination and differentiation (2-5). Once committed to the pituitary fate, the epithelium lining Rathke's pouch proliferates and differenti-

ates into pituitary-specific cell lineages that secrete peptide hormones critical for homeostasis, growth, and reproduction (6, 7). The mouse LIM homeobox gene *Lhx3* (also known as *mLim-3* and *P-Lim*) (8-10) and its *Xenopus* counterpart *Xlim3* (11) are expressed in the pituitary throughout development and in the adult. *Lhx3* is also expressed in the developing hindbrain, spinal cord, and pineal gland.

To analyze the function of *Lhx3*, we